M. Mariappan ✉
N.L. Parthasarathi
R. Ravindran
K. Lenin
A. Palanisamy

https://doi.org/10.21278/TOF.471032821
ISSN 1333-1124
eISSN1849-1391

IMPROVEMENT OF WELD BEAD CHARACTERISTICS IN GAS METAL ARC WELDING OF SA515 CARBON STEEL BY APPLYING ALTERNATING SHIELDING GAS FLOW TECHNIQUE

Summary

High service temperature of pressure vessel components necessitates the use of welded SA515 grade carbon steel components. The gas metal arc welding (GMAW) process using CO_2 as shielding gas is known for its undesirable spatter behaviour and inferior weld quality. The alternating shielding gas flow (ASGF) technique is proposed in this study using the shielding gases, viz. CO_2 and argon to overcome this difficulty. The welding current, stand-off distance, and shielding gas flow were all varied to improve the bead-on-plate profile geometry. The bead profile parameters such as depth of penetration, bead width, and bead height are considered as weld bead parameters. The following methods are used: correlation analysis, analysis of variance (ANOVA), modelling, and grey relational analysis (GRA). According to the findings, the welding current and ASGF are the most influential parameters impacting the weld bead characteristics. By increasing the welding current, the bead profile parameters increase linearly. The geometry of the bead profile was improved by using the GRA.

Key words: *GMAW; alternating shielding gas flow (ASGF); weld bead geometry; correlation; analysis of variance*

1. Introduction

SA515 Grade 70 carbon steel is used to manufacture components that are exposed to high temperatures, such as pressure vessels, furnaces, and coils. The gas metal arc welding (GMAW) process using CO_2 shielding gas was formerly applied to weld this material. The more weld spatter there is, the less stable the arc becomes. The ASGF technique turned out to be a promising approach to achieving transient arc characteristics. As a result, bead-on-plate experiments were carried out on this material preceding the bead-on-joint investigations. Furthermore, several traditional solutions for improving bead-on-plate profile characteristics were applied in the past. A study carried out on GTAW welding of DH36 grade as well as a cooled copper plate demonstrated that alternating the shielding gases, namely helium and argon, resulted in better weld bead characteristics. Appropriate pulsing frequency and flow rate resulted in a 13 % increase in the penetration of the weld [1]. The heat input and thermal pulse

frequency of the double-pulsed GMAW method were utilized to weld low-carbon steel to enhance the bead-on-plate profile geometry, and it was found that low heat input and high pulse frequency were appropriate to improve the bead profile geometry [2]. Robotic GMAW on mild steel was used in another approach to improve the bead-on-plate profile. The great depth of penetration was achieved with a welding speed of 10 mm/s, a voltage of 26 V, and a current of 210 A [3]. Welding on duplex stainless steel was also done with 100% CO_2 shielding gas. At a welding speed of 8mm/s, with a voltage of 30 V and current of 220 A, the depth of penetration of 1.899 mm, bead width of 13.38 mm and bead height of 3.295 mm were achieved [4]. The effects of helium and Ar/20% CO_2 shielding gas with various alternate frequencies on the depth/width ratio of the DH36 steel grade were investigated. The alternate frequency created a very narrow weld and deep penetration [5]. The performance of the traditional shielding gas (Ar and Ar + 67%He) and the alternating shielding gas (Ar: He) on the weld shape of austenite stainless steel 304 was investigated, and it was found that the alternative approach outperformed the traditional way [6]. Variable parameters were used to determine the best welding parameters for austenite stainless steel plates. Using an 87 A welding current, the depth of penetration of 2.654 mm, the height of 2.519 mm and the bead width of 6.496 mm were observed [7]. The use of Ar/20% CO_2 gas improved the depth of penetration in steel. The 1.6 mm penetration depth was reached by adjusting the alternate shielding gas frequency from 2 to 8 Hz and applying a 15 l/min gas flow rate, a voltage of 26 V, a current of 155 A, and a travel speed of 3 mm/s [8]. Using a gas flow rate of 15 l/min, a voltage of 20.7 V, a current of 126 A, and a travel speed of 6.4 mm/s, the Ar/10% He shielding gas mixture with alternating shielding gas frequency of 2 Hz was generated with a 10 mm weld width and 6 mm weld depth on the AA6082T6 aluminium alloy [9]. With a gas flow rate of 20 l/min, a voltage of 25 V, and a wire feed rate of 13.4 m/min, the Ar/He gas mixture with alternating shielding gas was created for welding the Al-Mg alloy plate at 8.5 mm weld width and 5.5 mm weld depth [10]. The design of the experiment was also utilized to improve the bead-on-plate profile qualities of mild steel. Weld currents ranging from 150 to 250 A and CO_2 shielding gas were used to accomplish the 4.02 mm depth of penetration, 0.891 mm bead height, and 7.53 mm bead width [11]. Artificial neural network models were used to improve the depth of penetration of cladded stainless steel, and it was found that the model had an improved depth of penetration [12]. Other approaches, such as vibration assistance welding [13], spin arc welding [14], and laser hybrid GMAW [15], enhance the bead profile characteristics. The cost calculations of welding structures, the study of the behaviour of welded joints under different temperatures and times, the study of cold cracking in underwater wet welding, characterization and mathematical modelling of arc welding, multi-objective optimization of welding process parameters and nugget formation of resistance spot welding were also carried out [16-21]. A few studies have reported the effect of current, stand-off distance, and alternative gas pulse frequency in terms of seconds, on the depth of penetration, bead width, and bead height of the GMAW welding of the SA515 grade 70 steel. Few studies have looked into the impact of different shielding gases on different steel grades.

This study aims to concentrate on improving the bead-on-plate profile geometry through experimental design. This study includes correlation analysis, analysis of variance, modelling, grey relational analysis, and a discussion of experimental results.

2. Materials and method

2.1 Equipment for an alternating supply of shielding gas flow

Figure 1 depicts a GMAW process with an ASGF attachment. Figures 1 (a) and (b) show a schematic diagram and an experimental setup, respectively. CO_2 and argon shielding gas are supplied separately to the GMAW torch by a gas alternator unit. A solenoid valve that is controlled by a timer changes the shielding gas flow regularly. Two-timer knobs of the shielding gas alternator must control a pre-set duration of the ASGF for each gas. A gas alternator is used

to transport two different gases to the GMAW torch from two separate gas cylinders. For other gases, the same flow rate is used. The frequency timing of the alternate supply of shielding gases is varied by seconds, ranging from 1 to 3 seconds.

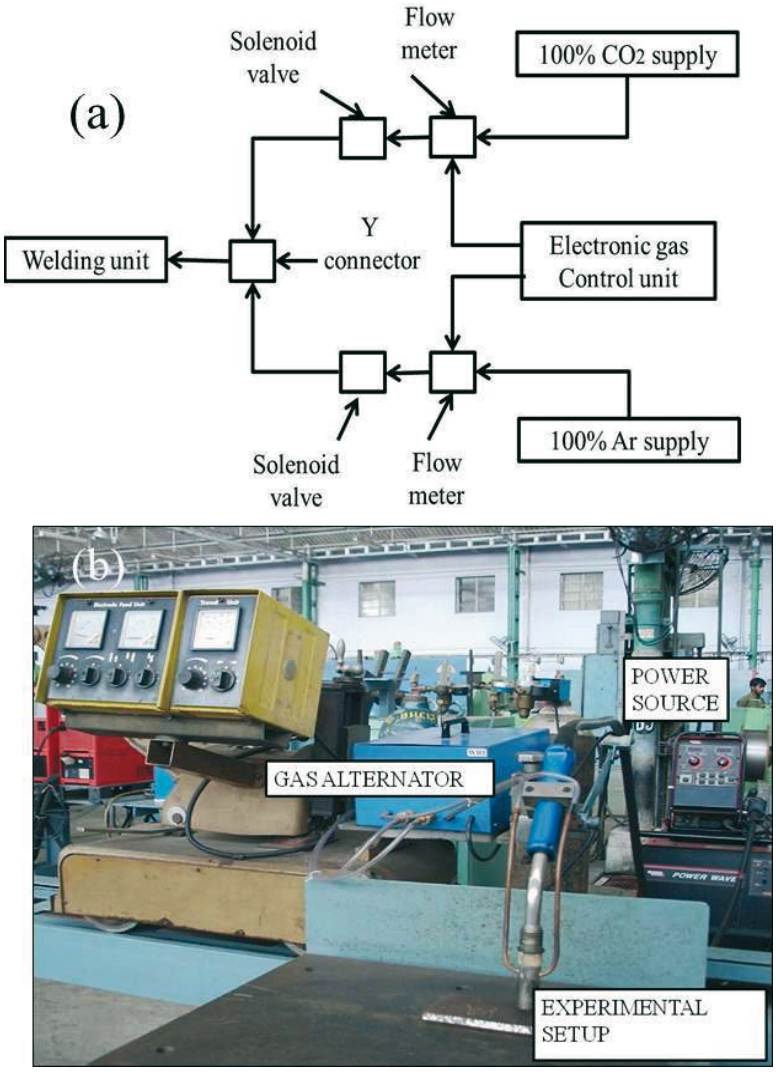

Fig. 1 (a) Schematic diagram of ASGF with electronic gas control unit (b) Experimental setup of GMAW with ASGF

2.2 Welding tests

Experimental materials include SA515 Gr 70 carbon steel and ER70S-6 electrode wire. Tables 1 and 2 show the chemical composition and mechanical properties of the base metal and the electrode wire, respectively. The welding process settings are chosen depending on the machine's capabilities and the advice of an industry specialist. The problems can also be seen when choosing the welding parameter, as illustrated in Table 3.

Table 1 Chemical composition of base metal and electrode wire

Elements (wt. %)	C	Mn	Si	S	P
Base metal SA515Gr70	0.31	1.2	0.15-0.4	0.04	0.035
Electrode wire: ER70S-6 (Ø1.2)	0.06 – 0.15	1.4 – 1.85	0.8 – 1.15	0.035	0.025

Table 2 Mechanical properties of base metal and electrode wire

Properties	Yield strength /MPa	Ultimate tensile strength /MPa	Elongation in %
Base metal SA515Gr70	260	485 - 620	21
Electrode wire: ER70S-6	452	538	24

Table 3 Selection of welding process parameters and problems observed

Levels	Current (*I*) /A	Stand-off distance (*SoD*) /mm	Gas pulse frequency timing (*GPF*) /s
1	90	12	1
2	190	16	2
3	290	18	3
Problem caused by lowering below limit	Machine limit	Selection based on thickness of sample and industrial experience	Selection by trail tests
Problem caused by increasing above limit	Solidification rate higher and poor surface finish	Selection based on thickness of sample and industrial experience	Selection by trail tests

2.3 Observation of responses

The profile projector was used to measure the depth of penetration (D), bead width (W), and bead height (H) after bead-on-plate welding tests have been carried out. Figure 2 shows a schematic of the specimen preparation. Figure 3 (a) and (b) show a schematic diagram of the bead-on-plate and the bead profile geometry, respectively. Table 4 depicts the design layout and responses. Figure 4 depicts the bead-on-plate profile for various currents.

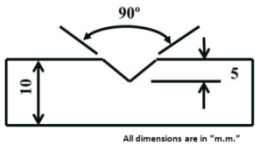

Fig. 2 Schematic diagram of specimen preparation

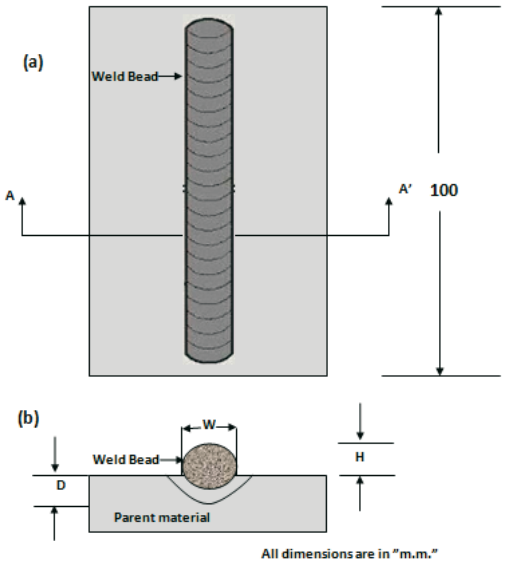

Fig. 3 Schematic diagram of: (a) bead-on-plate geometry (b) bead profile geometry

Table 4 Design layout and responses

Ex. no.	Design layout			Responses		
	Current /A	Stand-off distance /mm	Gas pulse frequency timing /s	Depth of penetration, *D* /mm	Bead width, *W* /mm	Bead height, *H* /mm
1	90	12	1	1.2	6.0	2.4
2	90	16	2	1.4	6.1	2.7
3	90	18	3	1.6	6.2	2.8
4	190	12	2	2.7	10.2	3.4
5	190	16	3	2.8	10.4	3.5
6	190	18	1	2.6	10.1	3.6
7	290	12	3	4.2	14.1	4.9
8	290	16	1	4.1	13.6	5.0
9	290	18	2	4.0	13.7	4.7

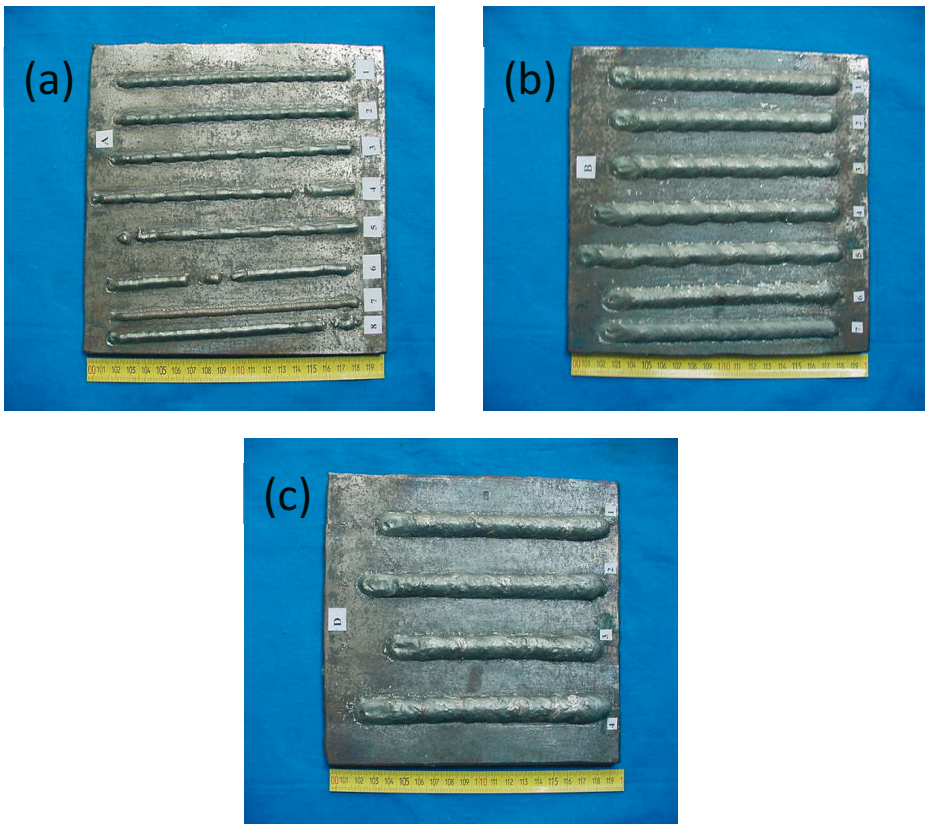

Fig. 4 Bead-on-plate profiles welded with a current of (a) 90 A, (b) 190 A and (c) 290 A

2.4 Grey relational analysis (GRA)

The GRA was the multi-objective optimization tool that was used to determine the best parameters. The reason for choosing this tool was that there were no specific constraints in the sample size selection. Also, distributed data is typically a simple computational problem when compared to other optimization tools [22]. This tool comprised six steps. The signal-to-noise ratio was used to identify a response in the first step. The second step was to normalise the signal-to-noise ratio of the response. The third step assigned the weightage to the response and computed the grey relational coefficient. The grey relational grade was calculated in the fourth step. The fifth step was to establish a rank. The GRA equations are given below.

Step 1: To select the S/N ratio based on the objective function

Larger is better; $^{S}/_{N}\ ratio = -10 * \log\left(\frac{1}{n}\right)\sum_{i=1}^{n} 1/y_{ij}^{2}$ (1)

Smaller is better; $^{S}/_{N}\ ratio = -10 * \log\left(\frac{1}{n}\right)\sum_{i=1}^{n} y_{ij}^{2}$ (2)

Here, n indicates the replicas; y_{ij} indicates the output values. The highest S/N ratio value will yield the optimal solution for each response.

Step 2: Normalization of the S/N ratio

$$N_i^*(k) = \frac{y_i(k) - y_i(k)}{y_i(k) - y_i(k)} \quad (3)$$

$$N_i^*(k) = \frac{max\ y_i(k) - y_i(k)}{y_i(k) - y_i(k)} \quad (4)$$

where i = 1…m; k =1, 2, 3…n; $y_i(k)$ = original sequence 1, 2, 3…27; $N_i^*(k)$ is the value after GRG, and $min_{yi}(k)$ and $max_{yi}(k)$ are the minimum and maximum value of $y_i(k)$, respectively.

Step 3: To calculate the grey relational coefficient

$$\epsilon_i(k) = \frac{\Delta\ min + \tau\Delta\ max}{\Delta_{oi}(k) + \tau\Delta\ max} \quad (5)$$

where $\epsilon_i(k)$ is the GRC; Δ_{oi} is the deviation between $N_o^*(k)$ and $N_i^*(k)$, $N_o^*(k)$ $^{N_o*(k)}$= the ideal (reference) sequence; $\Delta\ max$ =the highest value of $\Delta_{oi}(k)$ $^{\Delta_{oi}(k)}$; $\Delta\ min$= the lowest value of $\Delta_{oi}(k)$ $^{\Delta_{oi}(k)}$; τ is the assumed weightage.

Step 4: To calculate the grey relational grade

$$GRG = \left(\frac{1}{m}\right)\sum \epsilon_i(k) \text{----------} \quad (6)$$

In this case, m denotes the number of response variables. The higher the GRG, the closer the deviation between the actual experimental result and the ideal value to the ideal solution (i.e. optimum) is.

Step 5: To establish a rank.

Step 6: Using the GRG, to create a mean response.

3. Results and discussion

The bead-on-plate welds were performed on SA515 Gr 70 using an experimental design and an alternative shielding gas combination of CO_2 and argon. Responses such as depth of penetration, bead width, and bead height were measured after welding. Mean responses were calculated based on the design of the experiment to identify the statistically and physically significant parameters in the statistical analysis. Table 5 displays the mean responses. The maximum and minimum response values for each parameter were calculated and denoted as delta values. The delta value was used to calculate the rank for each parameter. The greater the delta value, the more significant the parameter. For improving the weld bead profile characteristics, the contributing percentages of each parameter were calculated. For evaluating model predictability, multiple regression models of the depth of penetration, bead width, and bead height were created. Multiple objective optimization techniques of the grey relational analysis were used to find the best process parameters and evaluate the results of the confirmation test. Finally, the current findings were compared to previous research findings.

3.1 Depth of penetration

The depth of penetration is the depth of the base and the filler material deposited in the weld pool. The depth of penetration is found to increase with an increase in the current, which is shown in Figure 5. Table 5 shows the most important parameter for the depth of penetration, which is current. This is because heat input is proportional to welding current and voltage and indirectly proportional to welding speed. Furthermore, increasing the heat input results in more preheating of the workpiece material during welding. Preheating has the effect of increasing melting and the rate at which heat spreads across the base metal. This is why the depth of penetration steadily increases as the welding current increases. In the paper [23], similar tendencies were identified. The depth of penetration decreases as the standoff distance between the tip of the nozzle and the workpiece increases. By raising the standoff distance, the arc length increases. As the arc length increases, it becomes unstable and the arc wanders. As a result, the constricted arc has a significant impact on the heat input to the work specimen. By raising the stand-off distance, a reduced depth of penetration is observed [24]. The weld pool as well as the surface are affected by the varying thermal conductivity of shielding gases. The depth of penetration increases as the gas pulse frequency timing is increased [25]. When the shielding gas pulse frequency is increased, the weld bead profile becomes homogeneous and smooth. When the current is increased, the depth of penetration improves by up to 96.585% (the range is from 1.4 mm to 4.1 mm).

Similarly, decreasing the stand-off distance improves the depth of penetration by 3.980% (the range varies from 2.253 mm to 2.347 mm), while increasing the gas pulse frequency improves the depth of penetration by 4.751% (the range varies from 2.273 mm to 2.387 mm). As a result, given a current input of 290 A, a stand-off distance of 12 mm, and an alternating shielding gas frequency timing of 3 seconds, the maximum depth of penetration is observed. In comparison to stand-off distance and shielding gas frequency timing, the welding current has a beneficial effect on the depth of penetration in this study. The impact of pulse parameters and of the alternating shielding gas flow approach on bead profile is investigated for improving bead profile characteristics due to arc oscillations and microstructural changes, as compared to other supporting evidence[25].

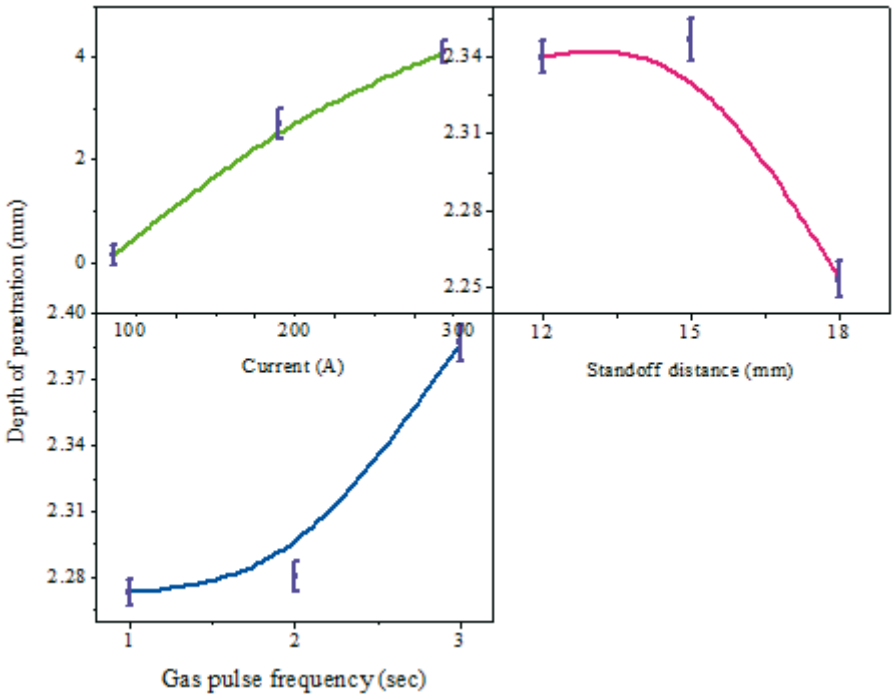

Fig. 5 Main effect plots for depth of penetration

Table 5 Mean responses

Levels	I /A	SoD /mm	GPF /s
(a) Depth of penetration			
1	1.400	2.340	2.273
2	2.700	2.347	2.280
3	4.100	2.253	2.387
Delta	3.960	0.093	0.113
Rank	1	3	2
Maximum	4.100	2.347	2.387
Minimum	1.400	2.253	2.273
IP	96.585	3.980	4.751
(b) Bead width			
1	6.10	10.10	9.90
2	10.23	10.03	10.00
3	13.80	10.00	10.23
Delta	7.70	0.10	0.33
Rank	1	3	2
Maximum	13.800	10.100	10.233
Minimum	6.100	10.000	9.900
IP	55.797	0.990	3.254
(c) Bead height			
1	2.63	3.57	3.67
2	3.50	3.73	3.60
3	4.87	3.70	3.73
Delta	2.23	0.17	0.13
Rank	1	2	3
Maximum	4.867	3.733	3.733
Minimum	2.633	3.567	3.600
IP	45.901	4.447	3.563
Delta = Maximum – minimum; Rank is formed based on the delta value			
Improvement percentage (IP) = ((maximum-minimum)/maximum) ×100			

3.2 Bead width

The breadth of the filler material deposited over the weld pool along the welded surface is referred to as the bead width. The bead width appears to expand as the current is increased, as shown in Figure 6. As a result of the higher current, the driving forces and heat input are enhanced. This is why the breadth of the beads is increased. The high current pulse heats the base metal, causing it to melt and be deposited over the weld pool, resulting in a great weld pool width. In addition, the greater current creates a high and stable directional arc, which reduces the electrode wander [25]. The bead width decreases as the standoff distance between the nozzle tip and the workpiece increases. Increasing the standoff distance has a minor effect on the fluctuation in the bead width. Due to the creation of a confined arc with heat delivered to the weld pool, the standoff distance has a significant impact on arc length. As a result, increasing the stand-off distance leads to a smaller bead width. In comparison to other data, there is a decrease in the melted surface depth and an increase in arc concentration in the lateral spread at specific spots when the standoff distance is increased. The constriction of the arc and heat delivered to the weld surface are found to be more evenly distributed across a larger area as the arc length is increased [26]. Because of the variable thermal conductivity of the shielding gas CO_2 and the argon effect, the bead width is increased by increasing the gas pulse frequency

timing. As a result, at high gas pulse frequencies, the bead width is greater. Arc configuration and bead shape are significantly impacted by the varying thermal conductivity of the shielding gases [27]. When the current is reduced, the bead width improves by up to 55.79% (the range varies from 13.8 mm to 6.1 mm). Similarly, increasing the stand-off distance and lowering the gas pulse frequency improves the bead widths by 0.99% and 3.25%, respectively. For a current input of 90 A, a stand-off distance of 12 mm, and a gas pulse frequency timing of 1 sec, the bead width is found to be minimal.

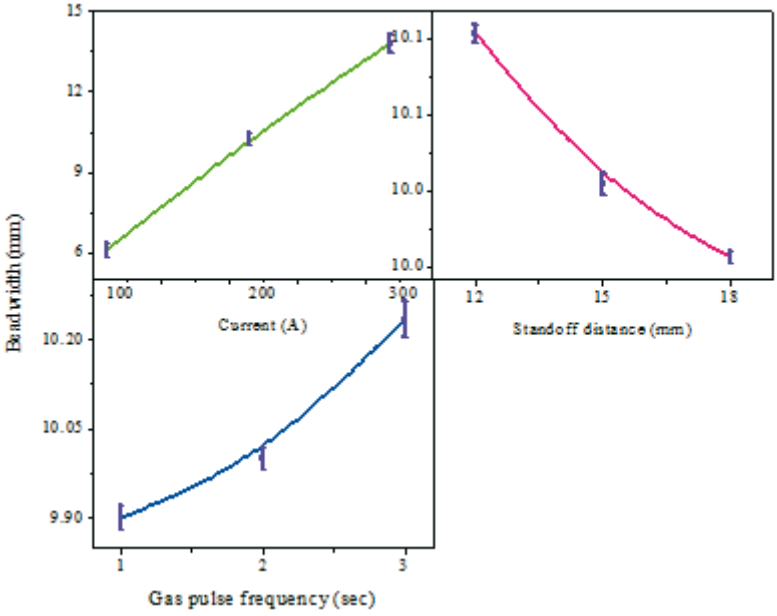

Fig. 6 Main effect plots for bead width

3.3 Bead height

The filler material placed on a welded pool at a height above the welded surface is known as bead height. The height of the beads was considerably affected by changes in current, standoff distance, and gas pulse frequency timing, as illustrated in Figure 7. Because of the more heat generated in the weld pool, a steady arc is created between the workpiece and the electrode. When the current is increased, the bead height increases. Welding current and arc voltage is directly proportional to arc energy, but welding speed is proportional indirectly. As a result, by lowering the current, the minimum bead height is achieved by using less driving force and heat input. The bead height decreases with the welding speed because the increased welding speed yields only lower heat input to the base metal per unit length, hindering also the filler metal deposition [28]. When the stand-off distance is increased, the bead height also increases due to the arc length variation. The bead height increase is a result of an inverse relationship between arc length and standoff distance. As a result, reducing the standoff distance lowers the bead height. A two-second gas pulse frequency is used to measure the minimum bead height. The bead height was found to be reduced for the two-second pulse frequency. Later, the bead height increased. The combinational thermal conductivity impact of CO_2 and argon shielding gas on weld pools causes fluctuation in the bead height. As a result, with the two-second gas pulse frequency timing, a lower bead height is observed. When the current is reduced, the bead height improves by up to 45.90% (with a range of 2.63 mm to 4.86 mm). Similarly, adjusting the standoff distance and gas pulse frequency increases the bead widths by 4.44% and 3.56%, respectively. As a result, for a current input of 90 A, a standoff distance of 12 mm, and a gas pulse frequency timing of two seconds, the bead height is found to be the smallest.

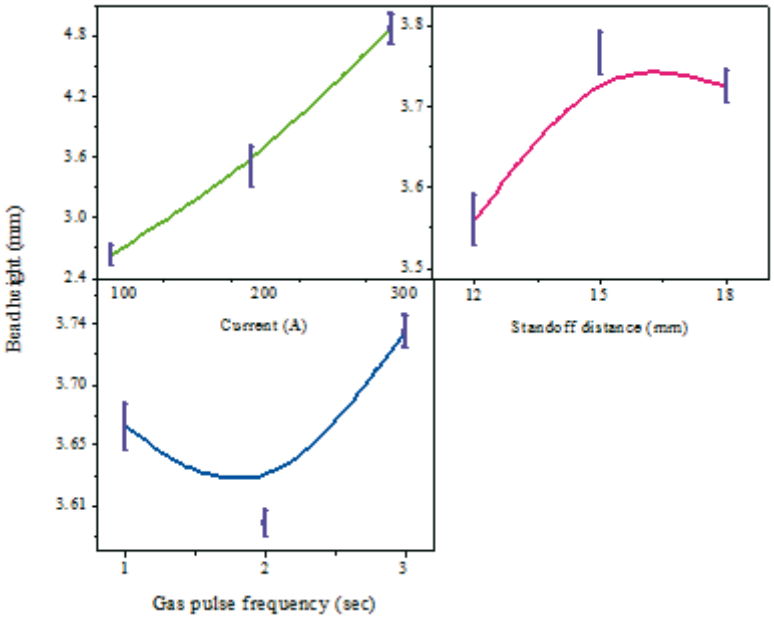

Fig. 7 Main effect plots for bead height

3.4 Correlation analysis

The depth of penetration, bead width, and bead height is used to evaluate the geometrical correlation of bead profiles. The influence of current, standoff distance and gas pulse frequency timing on penetration depth, bead width, and bead height is investigated. The depth of penetration, bead width, and bead height are all influenced by current. Among the numerous process variables, the welding current was the most influential variable. Based on the current, standoff distance, and gas pulse frequency timing, patterns in the bead profile features were established. Based on the current, a graph was created between the depth of penetration over the bead width and bead height, as shown in Figure 8(a). The graphs show that the depth of penetration is proportional to the width and height of the beads. By increasing the welding speed, the bead width and height were reduced in instantly [27]. Due to the increased heat input, the depth of penetration was generally enhanced when the current was increased. Based on the standoff distance, a graph was created showing the correlation between the depth of penetration and the bead width and bead height, as illustrated in Figure 8(b). The results show that the depth of penetration and bead width was gradually increased up to a precise limit, and then the bead width was considerably increased to maintain a constant depth of penetration. Due to insufficient heat input to the weld pool and molten metal flowing in the direction of the bead width, the depth of penetration must be maintained at a consistent level (welded surface). In addition, due to the diminishing arc stability and heat input to the weld pool, the depth of penetration and bead height are gradually increased up to a certain point, and then abruptly reduced while retaining the constant depth of penetration. Similarly, based on the gas pulse frequency timing, a graph is plotted between the depth of penetration and the bead width and bead height, as shown in Figure 8 (c). Due to the thermal conductivity of the shielding gas and more heat input to the weld zone, the depth of penetration, bead width, and bead height gradually increased when the gas pulse frequency was increased. The depth of penetration and the bead width have similar relationship tendencies [23].

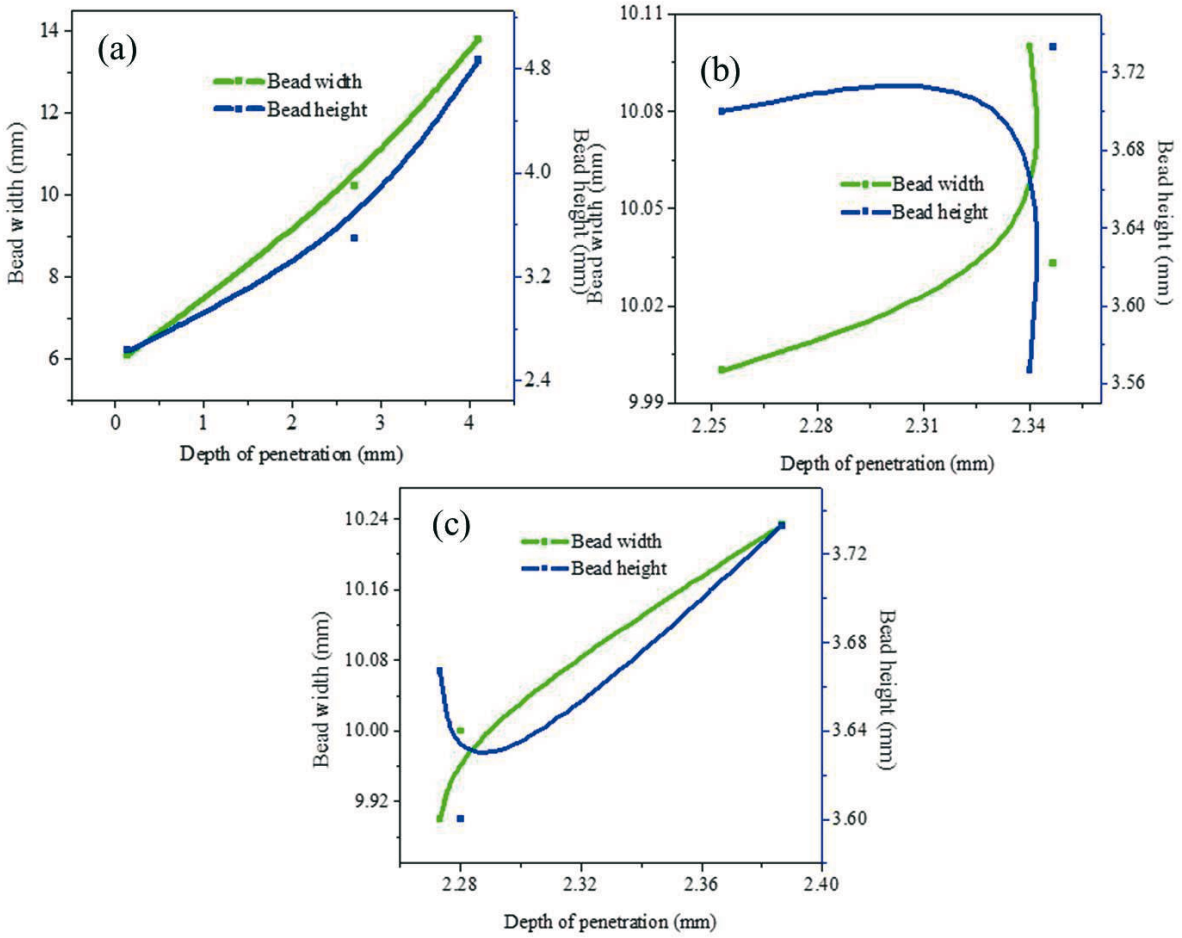

Fig. 8 Correlations between responses: (a) current, (b) standoff distance and (c) gas pulse frequency timing

3.5 Analysis of variance

The analysis of variance is used to find the most important variables that influence the quality of bead-on-plate welds. Table 6 shows the results of an analysis of variance (ANOVA) for depth of penetration, bead width, and bead height under a 95% confidence interval using the Minitab 18 statistical trial software. Three parameters and three levels are used to calculate the nine experiments. The number of experiments performed exceeds the degree of freedom of the experiment, which is determined by the number of factors and their associated levels. For the orthogonal array selections, the following two conditions are met: 1) The orthogonal array's degree of freedom is larger and equal to the degree of freedom of the experiment. 2) The orthogonal array's level is the same as the experiment's level. The number of independent aspects connected with the experimental design or factor is referred to as the degree of freedom. *S* is the standard deviation between the response values and the fitted values in the ANOVA table. The standard deviation is used to determine how accurately the model predicts the response. As a result, the smaller the S value, the more accurately the model describes the reaction. The model evaluates the variation in the response, which is represented as R-squared. The greater the R-squared number, the better the model matches the data. R-squared is a percentage that ranges from 0% to 100%. The percentage of variation in the response described by the model, adjusted for the number of predictors in the model compared to the number of observations, is known as adjusted R-squared. One minus the ratio of the mean squared error (MSE) to the mean square total yields adjusted R-squared (MS total). When comparing models with varying predictions, the adjusted R-squared is utilized. Lower S, higher R-squared, and

adjusted R-squared are used to determine which model is the best. The contribution percentage is also used to assess the most important factors that influence the response. It is determined by multiplying the ratio of each parameter's sequential sum of squares to the total sequential sum of squares by 100. The most important parameter, as determined by the sequential sum of the square test, is current. In addition, the welding current contributes a higher percentage to increasing the bead profile geometry. Experimental errors for bead profiles are less than 5%, which is considered acceptable. For bead profile geometries, the R-squared and the neighbouring R-squared are above 90%, and the experimental results were a good fit for prediction. The low S, high R-squared, adjusted R-squared, and predicted R-squared are also recognized, resulting in a better model summary for all responses.

Table 6 Analysis of variance for depth of penetration, bead width and bead height

Source	DoF	Seq SS	Adj SS	Adj MS	F	P	Inference	Contrib. percentage (%)
(a) Depth of penetration								
I	2	24.1952	24.1952	12.097	90732	0	Signific.	99.83
SOD	2	0.0163	0.0163	0.0081	61	0.016	Signific.	0.07
GPF	2	0.0243	0.0243	0.0121	91	0.011	Signific.	0.10
Error	2	0.0003	0.0003	0.0001				0.00
Total	8	24.236						100
S = 0.0115470 R-Sq = 100.00% R-Sq(adj) = 100.00%								
(b) Bead width								
I	2	89.096	89.096	44.548	5727.5	0	Signific.	99.77
SoD	2	0.016	0.016	0.008	1	0.5	Insignific.	0.02
GPF	2	0.176	0.176	0.088	11.29	0.081	Insignific.	0.20
Error	2	0.016	0.016	0.008				0.02
Total	8	89.302						100
S = 0.0881917 R-Sq = 99.98% R-Sq(adj) = 99.93%								
(c) Bead height								
I	2	7.6067	7.6067	3.8033	95.08	0.01	Signific.	98.02
SOD	2	0.0467	0.0467	0.0233	0.58	0.632	Insignific.	0.60
GPF	2	0.0267	0.0267	0.0133	0.33	0.75	Insignific.	0.34
Error	2	0.08	0.08	0.04				1.03
Total	8	7.76						100
S = 0.2 R-Sq = 98.97% R-Sq(adj) = 95.88%								
Error = Experimental error								
S = Standard deviation								
R-Sq = Coefficient of regression								
R-Sq (adj) = Adjusted coefficient of regression								
DoF = Degree of freedom								
Seq SS = Sequential sum of squares								
Adj SS = Adjusted sum of squares								
Adj MS = Adjusted mean square								
F = F-test								
P = P-value								

3.6 Modelling

The relationship between output and input process parameters is referred to as modelling. It is used to make more accurate predictions based on experimental data. Minitab 18 is used to create multiple linear regression equations. The R-squared and adjacent R-squared for responses are both above 90%, indicating that the experimental data will enable reliable prediction. According to the equations, the depth of penetration and bead width is proportional to the current and gas pulse frequency timing, and the stand-off distance is related to the current and gas pulse frequency timing indirectly. Furthermore, the current, stand-off distance, and gas pulse frequency timing are all directly related to the bead height. The coefficient value is used to identify these tendencies (positive and negative). From (7) to (9), the constructed regression equations are written as the equations below. Graphs showing the correlation between the experimental and the expected responses were created, as illustrated in Figure 9. For all of the responses, the experimental values were found to be quite near to the expected values. The models developed for penetration depth, bead width, and bead height all fit well.

Depth of penetration = - 1.375 + 0.0198 x current - 0.0121 x stand-off distance + 0.057x alternating shielding gas flow timing . (7)

R-Sq = 97.16%, R-Sq(adj) = 95.5%, S = 0.37

Bead width = 2.65 + 0.0385 x current - 0.0166 x stand-off distance + 0.167 x alternating shielding gas flow timing (8)

R-Sq = 99.79%, R-Sq(adj) = 99.66%, S = 0.19

Bead height = 1.23 + 1.12 x current + 0.0667 x stand-off distance + 0.0333 x alternating shielding gas flow timing (9)

R-Sq = 96.95%, R-Sq(adj) = 95.12%, S = 0.21

3.7 Determination of optimum process parameters

According to the results of the single objective optimization, different optimum process parameters can be observed in distinct responses. As a result, grey relational analysis (GRA) is used to determine unique optimum process parameters and optimize the bead profile geometry. The initial stage in the GRA is to convert the experimental results to a signal-to-noise ratio depending on the response targets. Maximization refers to the depth of penetration, whereas minimization refers to the width and height of the beads. Equation (1) is used to transform the experimental results of the depth of penetration into the signal-to-noise ratio. Equation (2) is used to transform the experimental result of bead width and bead height into a signal-to-noise ratio. The signal-to-noise ratio of the response is then translated into a normalised form in the second stage. Equation (3) is used to obtain a normalized form of depth of penetration. Equation (4) is used to obtain a normalized form of bead width and height. The depth of penetration, bead width, and bead height each have a weightage of 0.4%, 0.3%, and 0.3%, respectively.

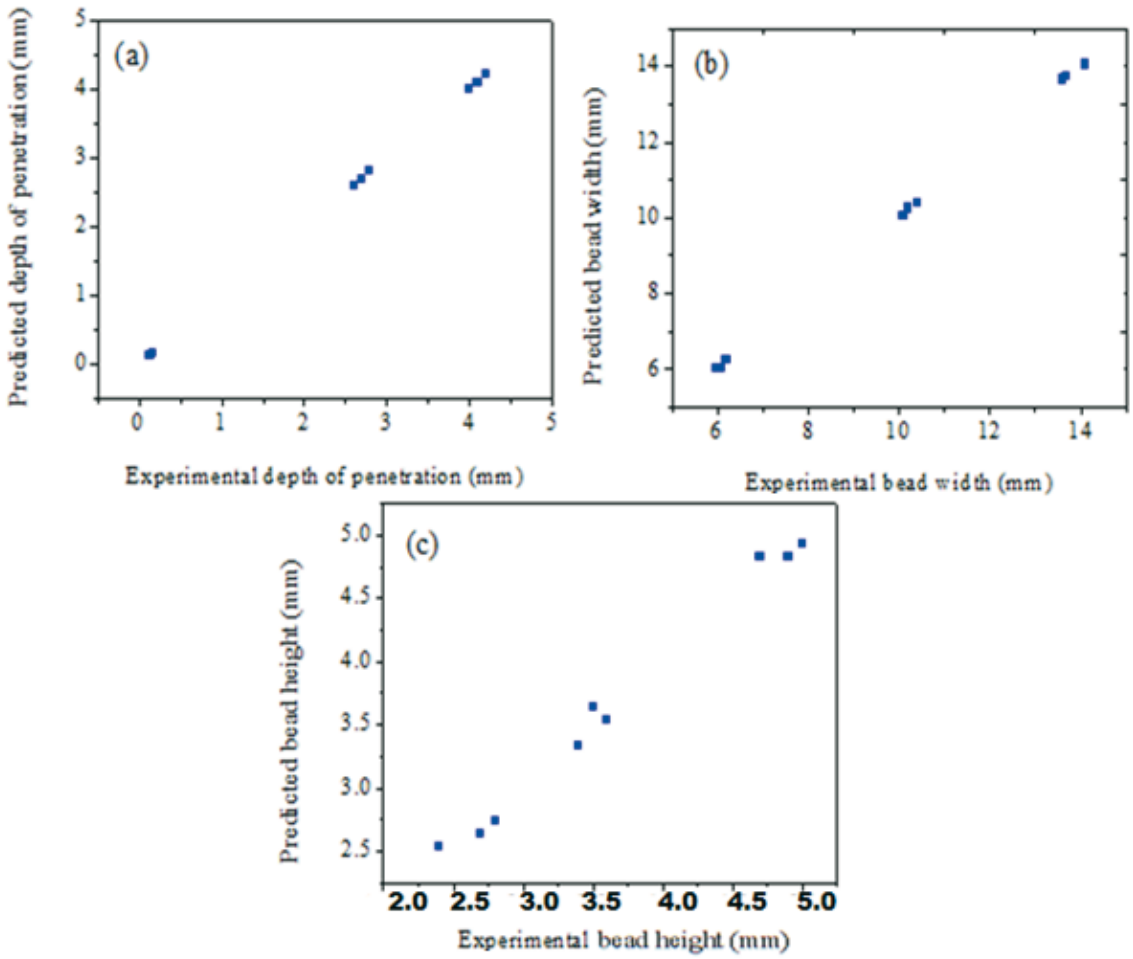

Fig. 9 Experimental responses with respect to predicted responses

The grey relational coefficient is determined in the third stage using Equation (5). Equation (6) is used to calculate the grey relational grade (GRG) in the fourth stage. The GRG is used to calculate the rank. The mean responses are calculated using the experimental design. The optimum parameters are determined by taking into account each parameter's greater mean GRG. The GRA computation is shown in Table 7. The average response for the GRG is shown in Table 8. The GRG trend curve is illustrated in Figure 10 and is dependent on the process parameter. The increased current and gas pulse frequency, as well as a shorter standoff distance, increase the bead profile. Table 9 shows the results of the analysis of variance for the GRG. According to the findings, the most influential aspect is current, which has a significant role in improving the bead profile properties. Because of the low standard deviation, high R-Sq, and R-Sq (adj) value, the model summary of the GRG is also a strong fit. The confirmation test is carried out in the best possible conditions, as illustrated in Table 10. The GRA is discovered to be employed to improve the bead profile properties.

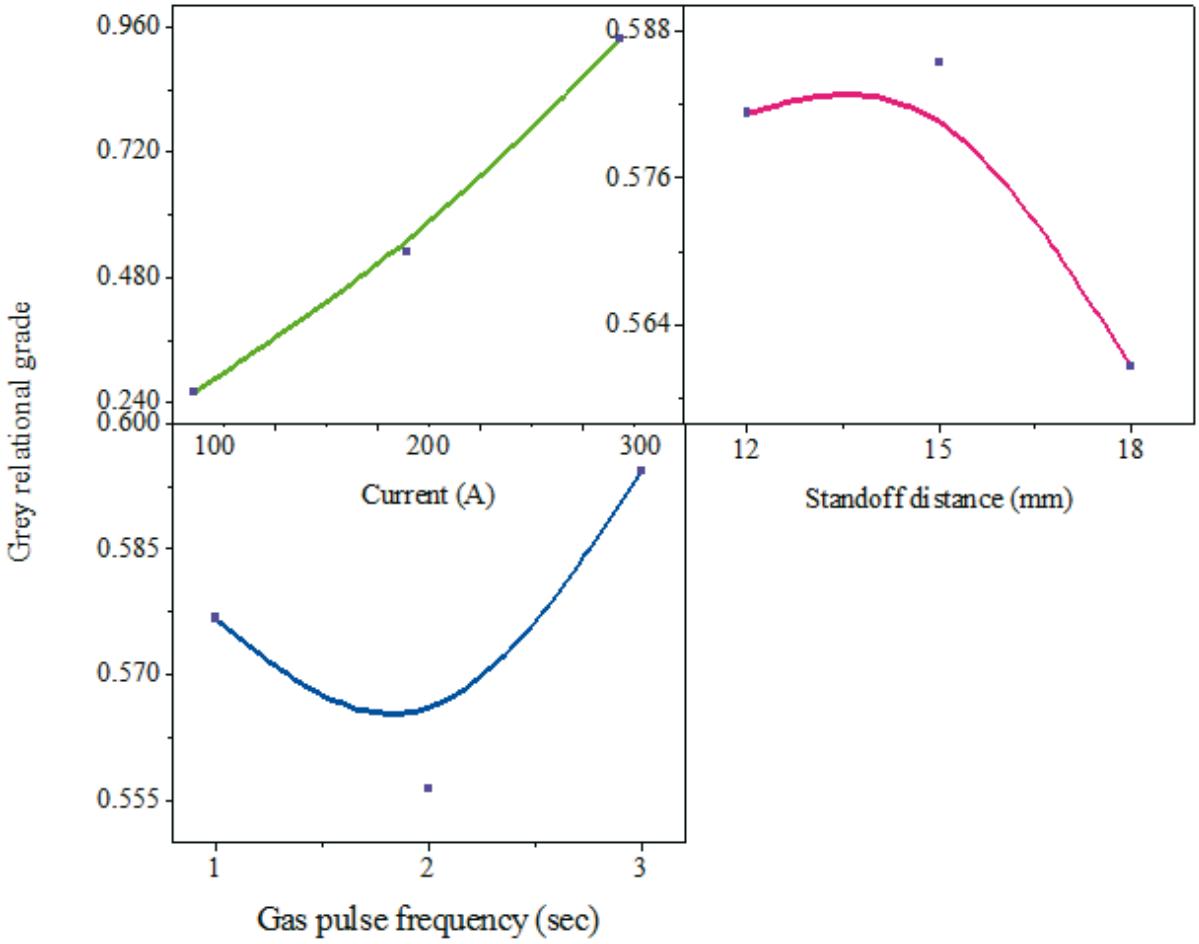

Fig. 10 Main effect plots for grey relational grade

3.8 Discussion and comparison with previous studies

The results of the current study and the previously published results are compared (see Table 11). In this study, the welding current is a crucial factor that impacts the depth of penetration, bead width, and bead height. When the welding current of more than 290 A was applied, higher solidification of molten metal and poor bead-on-plate welds were seen in the trial testing. As a result, the current was varied between 90 and 290 A in order to improve the bead-on-plate profile properties. Based on the alternating shielding gas flow, a comparison is made between the depth of penetration of SA515 Gr 70 and other metals, such as AISI 202 stainless steel [7], DH36 grade steel [8], AA6082T6 [30], Al-Mg [10], 904L SMSS [30], and carbon steel [31]. Because of the higher heat input, variations in the material properties, and variable shielding gases utilized, SA515 Gr 70 has a greater depth of penetration than other metals. The provided current and ASGF were determined to be the most influential parameters for optimizing the bead-on-plate profile geometry. Due to the differences in the thermal conductivity of the shielding gases, argon and CO_2 yielded better weld characteristics. In comparison to traditional improvement strategies, the ASGF method yields good results [30, 31]. Similarly, as compared to the prior results, the bead width and height are substantially improved in this study. The current depth of penetration, bead width, and bead height results are similar to those of the stainless steel grade [7]. As a result, the weld pool is alternately fed with argon and CO_2, which has been shown to improve the bead profile geometry.

Table 7 Grey relational calculations

Ex. no	S/N ratio			Normalised values			Grey relational coefficient			Grey relational grade	Rank
	D	W	H	D	W	H	D	W	H		
1	0.83	-15.56	-7.60	1.00	1.00	1.00	1.00	1.00	1.00	1.00	1
2	2.28	-15.71	-8.63	0.88	0.98	0.84	0.76	0.94	0.65	0.78	2
3	4.08	-15.85	-8.94	0.72	0.96	0.79	0.59	0.89	0.59	0.69	3
4	8.63	-20.17	-10.63	0.33	0.38	0.53	0.37	0.33	0.39	0.36	4
5	8.94	-20.34	-10.88	0.30	0.36	0.49	0.36	0.32	0.37	0.35	6
6	8.30	-20.09	-11.13	0.36	0.39	0.45	0.38	0.33	0.35	0.36	5
7	12.46	-22.98	-13.80	0.00	0.00	0.03	0.29	0.23	0.24	0.25	9
8	12.26	-22.67	-13.98	0.02	0.04	0.00	0.29	0.24	0.23	0.25	8
9	12.04	-22.73	-13.44	0.04	0.03	0.08	0.29	0.24	0.25	0.26	7

Table 8 Mean response for grey relational grade

Levels	Current /A	Standoff distance /mm	Gas pulsing frequency /s
1	0.82	0.54	0.54
2	0.36	0.46	0.47
3	0.25	0.44	0.43
Delta (max-min)	0.57	0.10	0.11
Rank	1	3	2
*Optimal parameters are: I1-SOD1-GPF1			

Table 9 Analysis of variance for GRG, using adjusted SS for tests

Source	DF	Seq SS	Adj SS	Adj MS		F	P	CP
I	2	0.5534	0.5534	0.2767		32.64	0.03	91.56
SOD	2	0.0164	0.0164	0.0082		0.97	0.508	2.72
GPF	2	0.0176	0.0176	0.0088		1.04	0.49	2.92
Error	2	0.0170	0.0170	0.0085				2.81
Total	8	0.6044						100
	S = 0.0920748 R-Sq = 97.19% R-Sq(adj) = 88.78%							

Table 10 Consolidated test results

Objective functions	Initial conditions	Optimal welding conditions	
		Prediction	Experiment
Levels	I1-SOD1-GPF1	I1-SOD1-GPF1	I1-SOD1-GPF1
Depth of penetration, mm	1.1	-	1.2
Bead width, mm	6.0	-	5.1
Bead height, mm	2.4	-	1.8
GRG	0.72	0.94	0.95
Improvement in % = 0.23			

Table 11 Comparison of present results with other studies

S. No	References	Materials/ method	*I* /A	*SoD* /mm	*GPF* /s	*D* /mm	*W* /mm	*H* /mm
1	Sivasakthivel P S, Sudhakaran R, 2018	AISI 202 stainless steel /AGPF	87	15	95% Ar and 5% CO_2	2.654	6.496	2.519
2	Campbell S W, Galloway A, and McPherson, N, 2012	DH36 grade steel / AGPF	155	-	2 – 8 Hz and Ar/20%CO_2	1.6	-	-
3	Sathiya P, Aravindan S, Jeyapaul R, 2010	AA6082T6/ AGPF	126	-	2 Hz and *Ar/10%He*	5	10	-
4	Kang B Y, Prasad Y K, Kang, M J, Kim, H J, 2009	Al–Mg /AGPF	-	-	2.2 Hz and Ar/He	5.5	8.5	-
5	Sathiya P, Aravindan S, Jeyapaul R, 2010	904L SMSS/conve ntional	-	-	-	3.36	11.01	3.33
6	Aloraier A, Almazrouee A, Shehata T, 2012	Carbon steel/convent ional	215-245			1.3	6.5	1.7
Present results								
	GRA	SA515 Gr 70/ AGPF	90	12	1 second and Ar and CO_2	1.2	5.1	1.8

4. Conclusion

The alternating flow of Argon and CO_2 shielding gases were used in place of argon in the arc welding process to improve the SA515 Gr 70 bead-on-plate profile geometry. Experiments were carried out using the design methods. The recorded data was utilized to determine the best bead geometry, i.e. the penetration depth, bead width, and bead height. The concluding remarks are as follows:

1. Increasing the current and alternating gas flow frequency accompanied by decreasing the stand-off distance enhanced the depth of penetration and bead width, whereas reducing the current and stand-off distance improved the bead height.
2. The correlation study revealed that as the welding current was increased, the depth of penetration, bead width, and bead height significantly increased. The current was the most important component impacting the bead profile geometry.
3. For prediction, multiple regression models were created and they were well-fitted. The bead profile geometry was optimized by applying the grey relational analysis.
4. When compared to traditional procedures, this alternate way of shielding gas flow provided a weld surface with enhanced bead profile properties.

REFERENCES

[1] Bitharas I, Campbell SW, Galloway AM, et al. Visualisation of alternating shielding gas flow in GTAW, Materials & Design, **2016**, 91, 424-431. https://doi.org/10.1016/j.matdes.2015.11.085

[2] Sen M, Mukherjee M, Singh SK, et al. Effect of double-pulsed gas metal arc welding (DP-GMAW) process variables on microstructural constituents and hardness of low carbon steel weld deposits. Journal of manufacturing processes, **2018**, 31, 424-439. https://doi.org/10.1016/j.jmapro.2017.12.003

[3] Ibrahim IA, Mohamat S A, Amir A, et al. The Effect of Gas Metal Arc Welding (GMAW) processes on different welding parameters. Procedia Engineering, **2012**, 41, 1502-1506. https://doi.org/10.1016/j.proeng.2012.07.342

[4] Mondal A, Saha M K, Hazra R, et al. Influence of heat input on weld bead geometry using duplex stainless steel wire electrode on low alloy steel specimens. **2016**, Cogent Engineering, 3(1). https://doi.org/10.1080/23311916.2016.1143598

[5] Campbell S W, Galloway, A M and McPherson, N A, Techno-economic evaluation on the effects of alternating shielding gases for advanced joining processes. Proceedings of the Institution of Mechanical Engineers, Part B: Journal of Engineering Manufacture, **2011**, 225(10), 1863-1872. https://doi.org/10.1177/0954405411408353

[6] Kang B Y, Prasad, YK, Kanget al. The effect of alternate supply of shielding gases in austenite stainless steel GTA welding. Journal of materials processing technology, **2009**, 209(10), 4722-4727. https://doi.org/10.1016/j.jmatprotec.2008.11.035

[7] Sivasakthivel P S and Sudhakaran R, Modeling and optimization of welding parameters for multiple objectives in pre-heated gas metal arc welding process using nature instigated algorithms. Australian Journal of Mechanical Engineering, **2018**, 1-12. https://doi.org/10.1080/14484846.2018.1472721

[8] Campbell S W, Galloway A, and McPherson, N, Artificial neural network prediction of weld geometry performed using GMAW with alternating shielding gases. Welding Journal, **2012**,91(6), 174S-181S.

[9] Campbell S W, Galloway, A M, McPherson N A, et al. Evaluation of gas metal arc welding with alternating shielding gases for use on AA6082T6. Proceedings of the Institution of Mechanical Engineers, Part B: Journal of Engineering Manufacture, **2012**, 226(6), 992-1000. https://doi.org/10.1177/0954405412439672

[10] Kang B Y, Prasad Y K, Kang, MJ, Kim, HJ et al. Characteristics of alternate supply of shielding gases in aluminum GMA welding. Journal of Materials Processing Technology, **2009**, 209(10), 4716-4721. https://doi.org/10.1016/j.jmatprotec.2008.11.036

[11] Srivastava S, and Garg RK, Process parameter optimization of gas metal arc welding on IS: 2062 mild steel using response surface methodology. Journal of Manufacturing Processes, **2017**, 25, 296-305. https://doi.org/10.1016/j.jmapro.2016.12.016

[12] Sreeraj P, and Kannan T, Modelling and prediction of stainless steel clad bead geometry deposited by GMAW using regression and artificial neural network models. Advances in Mechanical Engineering, **2012**, 4, p.237379. https://doi.org/10.1155/2012/237379

[13] Jose M J, Kumar S S, and Sharma A, Vibration-assisted welding processes and their influence on quality of welds. Science and Technology of Welding and Joining, **2016**, 21(4), 243-258. https://doi.org/10.1179/1362171815Y.0000000088

[14] Parthiban K, Shanmugam N.S, Sankaranarayanasamy K, and Vendan S A, Studies on spin arc welding process on the behavior of C1018 plates-an an insight into mechanical and metallurgical transformation. Materials Research Express, **2019**, 6(10), 106540. https://doi.org/10.1088/2053-1591/ab135d

[15] Pardal G, Martina F, and Williams S, Laser stabilization of GMAW additive manufacturing of Ti-6Al-4V components. Journal of Materials Processing Technology, **2019**, 272, pp.1-8. https://doi.org/10.1016/j.jmatprotec.2019.04.036

[16] Miler D, Hoić M, Birt D, et al, A comparison of welded structure cost calculation methods. Transaction of FAMENA, **2022**, 46(2), pp 85-96. https://doi.org/10.21278/TOF.462039122

[17] Bajramović E, Gačo D, Islamović F, Behaviour of High-Alloy Steel Welded Joints of Steam Pipelines under the Influence of Temperature and Exploitation Time. Transactions of FAMENA, **2022**, 46 (3), pp 103-113. https://doi.org/10.21278/TOF.463039822

[18] Garasic I., Krajl S., Kozuh S.: Investigation into cold cracking in underwater wet welding of API5L X70 steel. Transactions of FAMENA, **2009**, vol. 33, 3, pp 25-34.

[19] Urevc, Janez; Koc, Pino; Štok, Boris. Characterization of material parameters used in the mathematical modelling of arc welding and heat treatment processes. Transactions of FAMENA, **2011**, Vol. 35 Issue 4, pp. 1-14.

[20] Devanathan C Sureshbabu A S Multi Objective Optimization of Process Parameters by Firefly Algorithm during the Friction Stir Welding of Metal Matrix Composites. Transactions of FAMENA, **2021**, 45(1), pp. 117-128. https://doi.org/10.21278/TOF.451018520

[21] Akkuş A. Nugget formation effects in resistance spot welded different steel sheets Transactions of FAMENA, **2017**, 41(4), pp.71-76. https://doi.org/10.21278/TOF.41407

[22] Yao P, Zhou K, Lin H, Xu, Z et al. Exploration of weld bead forming rule during double-pulsed GMAW process based on grey relational analysis. Materials, **2019**, 12(22), p.3662. https://doi.org/10.3390/ma12223662

[23] Sudhakaran R, VelMurugan V, Senthil Kumar K M et al. Effect of welding process parameters on weld bead geometry and optimization of process parameters to maximize depth to width ratio for stainless steel gas tungsten arc welded plates using genetic algorithm. European Journal of Scientific Research, **2011**, 62(1), 76-94.

[24] Balasubramanian V, Lakshminarayanan A K, Varahamoorthy R, et al. Understanding the parameters controlling plasma transferred arc hardfacing using response surface methodology. Materials and Manufacturing Processes, **2008**, 23(7), 674-682. https://doi.org/10.1080/15560350802316744

[25] Pal K, and Pal S K, Effect of pulse parameters on weld quality in pulsed gas metal arc welding: a review. Journal of materials engineering and performance, **2011**, 20(6), pp.918-931. https://doi.org/10.1007/s11665-010-9717-y

[26] Deshmukh DD, and Kalyankar VD, Deposition Characteristics of Multitrack Overlay by Plasma Transferred Arc Welding on SS316Lwith Co-Cr Based Alloy-Influence of process parameters. High-Temperature Materials and Processes, **2019**, 38, 248-263. https://doi.org/10.1515/htmp-2018-0046

[27] TernerM, BayarsaikhanTA, Hong, H U, et al. Influence of gas metal arc welding parameters on the bead properties in automatic cladding. Journal of Welding and Joining, **2017**, 35(1), 16-25. https://doi.org/10.5781/JWJ.2017.35.1.16

[28] Gupta S K, Mehrotra S, Raja A R, et al. Effect of welding speed on weld bead geometry and percentage dilution in gas metal arc welding of SS409L, Materials Today: Proceedings, **2019**, 18, 5032-5039. https://doi.org/10.1016/j.matpr.2019.07.497

[29] Tseng K H, and Wang NS, Research on bead width and penetration depth of multicomponent flux-aided arc welding of grade 316 L stainless steel. Powder Technology, **2017**, 311, 514-521. https://doi.org/10.1016/j.powtec.2017.02.005

[30] Sathiya P, Aravindan S, Jeyapaul R, et al. Optimizing the weld bead characteristics of super austenitic stainless steel (904L) through grey-based Taguchi method, Multidiscipline Modeling in Materials and Structures, **2010**, 6, 2, 206 - 213. https://doi.org/10.1108/15736101011067993

[31] Aloraier A, Almazrouee A, ShehataT,et al. Role of welding parameters using the flux-cored arc welding process of low alloy steels on bead geometry and mechanical properties. Journal of materials engineering and performance, **2012**, 21(4), 540-547. https://doi.org/10.1007/s11665-011-9948-6

Submitted: 29.7.2021

Accepted: 12.01.2023

M. Mariappan*
Mookambigai College of Engineering, Pudukkottai, Tamil Nadu, India
N.L. Parthasarathi
Indira Gandhi Centre for Atomic Research - Kalpakkam, Tamil Nadu, India
R. Ravindran
Akshaya College of Engineering and Technology, Coimbatore, Tamil Nadu, India
K. Lenin
K. Ramakrishnan College of Engineering, Tiruchirapalli, Tamil Nadu, India
A. Palanisamy
Surya Engineering College, Erode, Tamil Nadu, India
*Corresponding Author:
mmariappan1809@gmail.com